Electronic and optical properties of two-dimensional heterostructures and heterojunctions between doped-graphene and C- and N-containing materials

Van der Waals DFT applied to C- and N-containing Two-dimensional Materials-based Heterostructures and Heterojunctions

A. Bafekry[a,*], D. Gogova[b], C. Nguyen[c], M. M. Fadlallah[d], M. Ghergherehchi[e], M. Faraji[f], M. Oskoeian[g]

[a]*Department of Radiation Application, Shahid Beheshti University, Tehran, Iran*
[b]*Department of Physics, University of Oslo, P.O. Box 1048, Blindern, Oslo, Norway*
[c]*Department of Materials Science and Engineering, Le Quy Don Technical University, Ha Noi 100000, Vietnam*
[d]*Department of Physics, Faculty of Science, Benha University, 13518 Benha, Egypt*
[e]*College of Electronic and Electrical Engineering, Sungkyun Kwan University, Suwon, Korea*
[f]*Micro and Nanotechnology Graduate Program, TOBB University of Economics and Technology, Sogutozu Caddesi No 43 Sogutozu, 06560, Ankara, Turkey*
[g]*Department of Physics, University of Guilan, 41335-1914 Rasht, Iran*

Abstract

The electronic and optical properties of vertical heterostructures (HTSs) and lateral heterojunctions (HTJs) between (B, N)-codoped graphene (dop@Gr) and graphene (Gr), C_3N, BC_3 and h-BN monolayers are investigated using van der Waals density functional theory calculations. We have found out all considered HTSs are energetically and thermally feasible at room temperature, therefore they can be synthesized experimentally. The dop@Gr/Gr, BC_3/dop@Gr and BN/dop@Gr HTSs are semiconductors with a direct bandgap of 0.1 eV, 80 meV and 1.23 eV, respectively, while the C_3N/dop@Gr is a metal because of the strong interaction between dop@Gr and C_3N layers. On the other hand, the dop@Gr-Gr, and BN-dop@Gr HTJs are semiconductors, whereas the C_3N-dop@Gr and BC_3-dop@Gr HTJs are metals. The HTSs proposed can enhance the absorption of light in the whole wavelength range as compared to Gr and BN monolayers. The applied electric field or pressure strain changes the bandgaps of the HTSs and HTJs, indicating that these HTSs are highly promising for application in nanoscale multifunctional devices.

Keywords: Heterostructures and heterojunctions, Graphene, C_3N, BC_3 and *h*-BN monolayers carbon nitride, Electro-optical properties, Electric field, Strain engineering, First-principle calculations

1. Introduction

After the successful synthesis of graphene and owing to its zero bandgap, several two-dimensional materials (2DM) with extremely intriguing properties have been proposed and investigated towards a new generation for nanoelectronics, optoelectronics and valleytronics [1]. Most 2DMs possess semiconducting nature with the sizable bandgap of $\sim$ 0.7 eV [2–4]. Such small band gap of 2DM gives rise to various applications, such as ultra fast IR photodetectors [5, 6], FETs [7, 8] and so forth. Nowadays, several novel 2DMs, such as transition metal dichalcogenides (TMDCs)[9–11], phosphorene analogues [12–14], graphitic carbon nitride [15, 16] have been received more consideration because of their interesting properties and wide applications. Unfortunately, these 2DMs also possess some drawbacks that may limit their potential applications. For instance, the wide bandgap ($\sim$ 6 eV) [17] of hexagonal boron nitride (*h*-BN) hinders its applications in photocatalysis. Furthermore, the low carrier mobility (200 cm^2/Vs) [18] at room temperature of MoS_2 limits its applications in nanoelectronics. Therefore, the search for common strategies that can use to overcome such limitations in novel 2DM is an important challenge in the scientific community alongside the search for novel 2DM.

Recently, atomic doping has been proven to be the main approach for modification of the physical and optical properties of 2DMs. Nowadays, the formation of the porous graphitic boron nitrides, such as C_2N, C_3N_4, and C_3N monolayers gives rise to the existence of novel interesting phenomena that may not hold in perfect materials, such as on/off current ratio [19], high thermal conductivity [20]. As an example, Mahmood and coworkers predicted the high on/off ratio of 10^7 of C_2N monolayer [19], showing a great interest for field-effect transistors. On the other hand, the formation of single layer C_3N_4 gives rise to a promising candidate for hydrogen generation [21, 22]. Very recently, a newly fabricated 2D C_3N material has been synthesized experimentally [23, 24]. It has been predicted that this material can be considered as a promising candidate for field-effect transistors due to its small bang gap (0.39 eV) and high on/off ratio of 5.5×10^{10} [24]. The adjustable electronic and optical features of such material under strain [25–27], electric field [25, 28], doping [29–32], functionalization [33–35], defects [36–39] and the number of stacking layers [40–44] makes it more attractive for various fields of future applications, such as Li-ion battery [45], metal-free catalyst [29, 46], short channel transistors [26], and gas sensors [47].

The purpose of our paper is to study the electronic and optical properties of doped graphene with graphene, C_3N, BC_3 and *h*-BN heterostructures (HTSs) and heterojunctions (HTJs). Interestingly, the B-N codoped graphene monolayer with a dopant

*Corresponding author
Email address: bafekry.asad@gmail.com (A. Bafekry)

concentration of 12.5% in the hexagonal configuration is a direct bandgap semiconductor with 1.3 eV bandgap. The computational methods are introduced in section II, the optimized structures and the electronic properties of pristine monolayers and doped graphene sheet, and heterostructures are discussed in sections III and IV, respectively. The optical properties of the HTSs and HTJs are addressed in section IV. The effects of applied electric fields and pressures on electronic structures of HTSs and HTJs are tackled in sections V and VI, respectively. At the end the summary and conclusions of this study is presented in section VII.

2. Computational Methods

The linear combination of multiple pseudoatomic orbitals implementation of density functional theory in the ab initio simulation package OpenMX package [48] is used to study the structures optimization, structure stabilities, electronic and optical properties. The Perdew-Burke-Ernzerhof generalized gradient approximation, the cutoff energy of 300 Ry, and a 23 × 23 × 1 of the Monkhorst-Pack k-mesh [49] are utilized. Atomic forces are converged to 1 meV/Å. A large vacuum layer of 20 Å along the z axis is considered to avoid the adjacent layers interactions in monolayers, HTSs, and HTJs. The empirical dispersion method of the DFT-D2 [50] is employed to get a clear picture in view of van der Waals interactions. To analyze the optical properties, using SIESTA package [51], the absorption coefficient [52, 53] $\alpha(\omega) = \sqrt{2}\omega\sqrt{\sqrt{\varepsilon_1^2(\omega)+\varepsilon_2^2(\omega)}-\varepsilon_1(\omega)}$, is calculated, where ε_1 and ε_2 are the real and imaginary parts for the dielectric function at angular frequency ω, respectively. The Kramers-Kronig relation is used to get $\varepsilon_1(\omega)$. and the transmission matrix between the occupied bands and unoccupied bands is calculated to obtain $\varepsilon_2(\omega)$. Ab initio molecular dynamics (AIMD) simulations were also carried out to examine the thermal stability of monolayer by using (4 × 4 × 1) supercell at room temperature (300 K) with total simulation time of 3 ps with 2 fs time steps.

3. Pristine monolayers and (B,N) codoped graphene

Figs. S1(a-d) of the supplementary information (SI) shows the electronic structure of graphene (Gr), C_3N, BC_3 and h-BN (BN) monolayers. The optimized structures of these monolayers are shown in the top of panel. We find the lattice parameters of the primitive unit cell are 2.46 Å for Gr, 4.86 Å for C_3N, 5.17 Å for BC_3, and 5.06 Å for BN which is in a good agreement with previous results [54–59]. All monolayers have planar structures with calculated C-C bond lengths of 1.42 Å for Gr, 1.40 Å for C_3N, and 1.42 for BC_3. While the N-C, B-C, and B-N bond lengths are, respectively, 1.40 Å for C_3N, 1.56 Å for BC_3, and 1.46 Å for BN. The density of states (DOS) of studied monolayers is shown in Fig. S1(e). The electronic band structure and the DOS shows that the Gr is a semimetal with a zero bandgap and the valence and conduction bands crossing with linear dispersions which and locate at the K-point. The

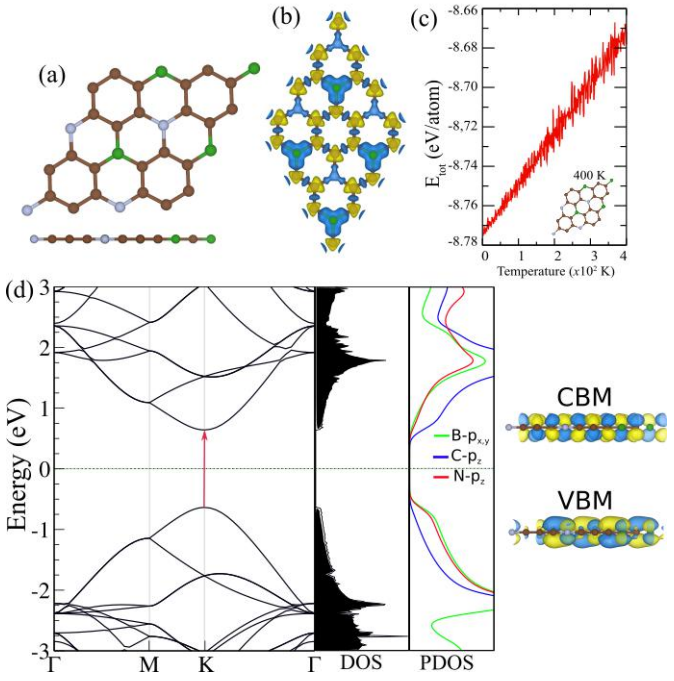

Figure 1: (a) Optimized structure of (B,N) codoped graphene, (b) the charge density and (c) Ab initio molecular dynamics at 400 K for dop@Gr. The top view of optimized structure at 400 K is displayed in the inset. The blue and yellow colors represent the charge accumulation and depletion, respectively. (d) electronic band structure and corresponding density of states (DOS) and partial DOS (PDOS) of dop@Gr. The energy is calculated relative to the Fermi energy. The charge densities of the VBM and CBM states are displayed in the right panel.

C_3N and BC_3 have indirect bandgap of 0.4 eV, and 0.7 eV, respectively. Notice that the valence band maximum (VBM) and conduction band minimum (CBM) are located at the Γ and the M points, respectively. The last monolayer is BN which has a direct bandgap of 1.45 eV and the CBM and VBM are located at Γ point. Our obtained bond lengths and electronic structures are in good agreement with the previous study [54–59].

For (B,N) codoped graphene (dop@Gr), the B and N substitutional dopants with 12.5% concentration in hexagonal patterns are used to open the bandgap in graphene monolayer (dop@Gr). The hexagonal pattern is similar to the hexagonal pattern in C_3N and BC_3.

The optimized structure of dop@Gr is depicted in Fig. 1(a). the lattice parameter is calculated 10.024 Å, while the C-C, C-B and C-N bond lengths are 1.42, 1.48 and 1.46 Å, respectively. The bond angle between atoms is ∼ 120°, displaying the characteristics of sp^2-hybridization. The dop@Gr is still a planar structure due to the weak effect of codoping. The difference charge density of dop@Gr is shown in 1(b), where the blue and yellow regions represent the charge accumulation and depletion, respectively. The cohesive energy were calculated using the following formula: $E_{coh} = \frac{E_{tot}-\sum n_B E_B + sumn_N E_N}{N}$ where E_{tot}, E_B (E_N) and n_B (n_N) represents the total energy of dop@Gr, atomic energy and the amount of B (N) atoms, and N is the total number of atoms present in the Gr monolayer, respectively. For the dop@Gr with 12.5% concentration, the cohesive energy

Table 1: The lattice constant **a** (Å), the bond lengths between C-C (d_{CC}), N-C (d_{NC}), B-C (d_{BC}), and B-N (d_{BN}) atoms (the numbers outside (inside) the parenthesis refer to the distances (Å) in the top (bottom) layer), the interlayer distance between two layers (h) (Å), the binding energy (E_b) (meV), electronic states (ES) are specified as metal (M) and semiconductor (SC), calculated bandgap within PBE (E_g^{PBE}) (eV)), and the VBM and CBM positions for considered HTSs.

Sys.	**a**	d_{CC}	d_{NC}	d_{BC}	d_{BN}	h	E_b	ES	E_g^{PBE}	VBM/CBM
Gr/dop@Gr	9.931	1.413 (1.433)	1.442	1.466	-	3.335	-80.09	SC	0.1	K
C_3N/dop@Gr	9.849	1.402 (1.424)	1.428 (1.418)	1.452	-	3.326	-73.85	M	–	–
BC_3/dop@Gr	10.167	1.440 (1.405)	1.485	1.503 (1.529)	-	3.334	-67.12	SC	0.1	Γ/K
BN/dop@Gr	9.997	1.421	1.453	1.476	(1.442)	3.333	-84.92	SC	1.24	K

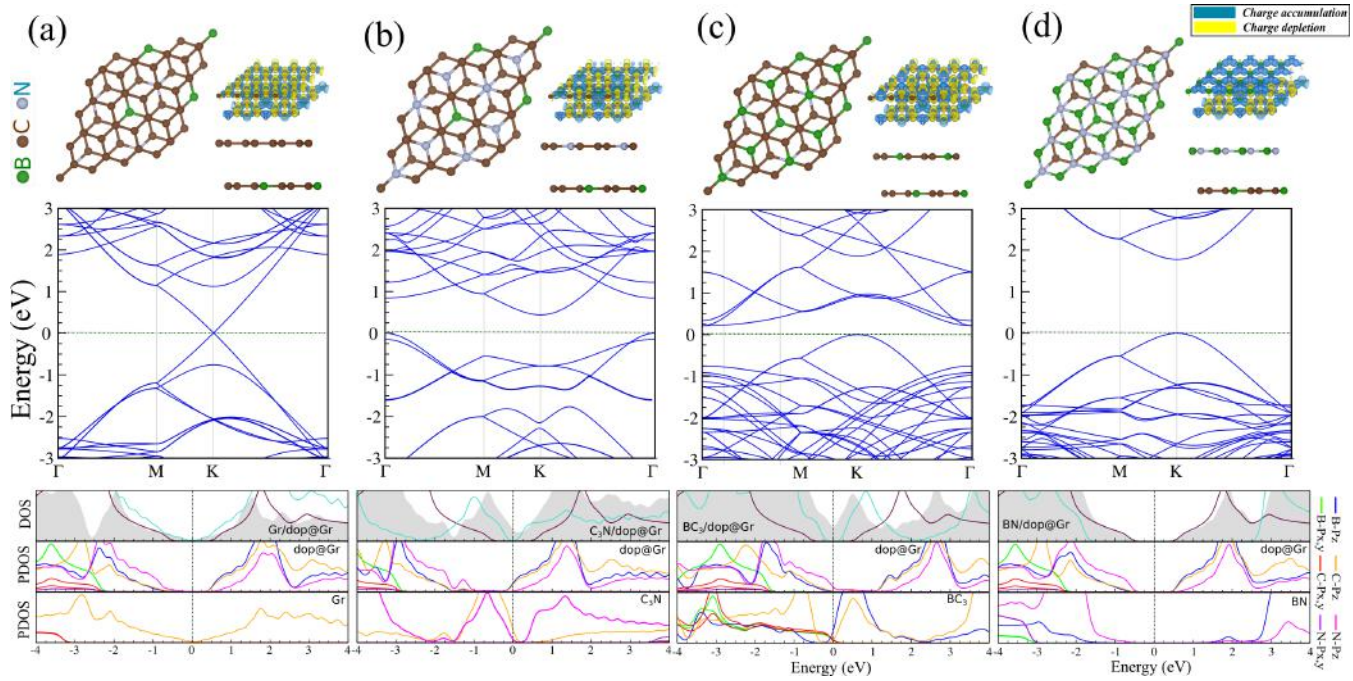

Figure 2: Optimized structures (top) and electronic band structure (middle) and DOS and PDOS (bottom) of (a) Gr/dop@Gr, (b) C_3N/dop@Gr, (c) BC_3/dop@Gr and (d) BN/dop@Gr HTS. The energy is calculated relative to the Fermi energy. Difference charge density is shown in the right of the optimized structures.

is calculated to be E_{coh}=-7.70 eV/atom. The Ab initio molecular dynamics at 400 K of dop@Gr is shown in Fig. 1(c). The top view of optimized structure at 400 K is illustrated as the inset figure. The thermal dynamic investigations are started with the optimized structure at 0 K. The temperature was increased to 400 K within 2 ps. Apart from minor distortions, the crystal structure of the dop@Gr is preserved and has a thermal stability at 400 K. The electronic band structure with the corresponding DOS, and projected DOS (PDOS) of dop@Gr is shown in Fig. 1(d). The dop@Gr is a semiconductor with a direct bandgap of 1.3 eV at the K-point, while the charge densities of VBM and CBM are shown in the right panel. The B-$p_{x,y}$ and N-p_z orbital states are dominated in the VBM, while C-p_z orbital states are dominated in the CBM.

4. Heterostructure

The vertical/lateral stacking of the single layer of graphene, C_3N, BC_3 and BN with dop@Gr does not affect the planar of the sheets due to the small mismatch (1.2 %-2.2 %) of the heterostructures lattice parameter. The lattice mismatch (δ) is defined as $\delta = \frac{|a_{up}-a_{dn}|}{a_{dn}} \times 100\%$, where a_{up} and a_{dn} represent the lattice constants of upper and down layers, respectively. The lattice mismatch between dop@Gr with C_3N, Gr, C_3N, BC_3 and BN monolayers are determined to be 1.20%, 2.40%, 3.81% and 1.60%, respectively. Our results show that the minimum energy configuration is an AB-stacking arrangement. The binding energy (E_b) of the HTSs is analyzed using: $E_b = E_{tot} - E_{dop@Gr} - E_X$ where E_{tot}, $E_{dop@Gr}$, and E_X are the total energy of HTS, dop@Gr monolayer, and other layers ($X = C_3N, BC_3$, and BN), respectively. The binding energy as a function of the interlayer distances is presented in Fig. S2. The equilibrium distances of Gr/dop@Gr, C_3N/dop@Gr, BC_3/dop@Gr, and BN/dop@Gr are 3.335, 3.326, 3.334, and 3.333 Å, respectively, and their binding energies are −80, −73, −67, and −85 meV, respectively. The negative energies refer to the stabilities of HTSs. The BN/dop@Gr is energetically more favorable than the other HTSs. Interestingly, the negative binding energy in the interlayer distances from 2.3 to 4.5 Å without bonding contact between the layers indicates the stability of the constructed bilayer which means these HTSs are energetically stable and can be synthesized experimentally, which is a very important result in terms of design of novel devices.

The top and side views of optimized structures (top) and electronic band structure (bottom) of Gr/dop@Gr, C_3N/dop@Gr, BC_3/dop@Gr and BN/dop@Gr HTS, respectively, are shown

Table 2: The lattice constant **a** (Å), the bond lengths between C-C (d_{CC}), N-C (d_{NC}), B-C (d_{BC}), and B-N (d_{BN}) atoms (all bond lengths are given in Å), electronic states (ES) are specified as metal (M) and semiconductor (SC), calculated bandgap within PBE (E_g^{PBE} (eV)), and the VBM and CBM positions for HTJs considered.

Sys.	**a**	**b**	d_{CC}	d_{NC}	d_{BC}	d_{BN}	ES	E_g^{PBE}	VBM/CBM
Gr/dop@Gr	19.869	9.929	1.434 (1.434)	1.444	1.477	-	SC	0.4	Y-Γ/Y-Γ
C_3N/dop@Gr	19.690	9.844	1.407 (1.401)	1.443 (1.4425)	1.460	-	M	-	-
BC_3-dop@Gr	20.337	10.142	1.396 (1.371)	1.418	1.446 (1.488)	-	M	-	-
BN-dop@Gr	20.133	9.976	1.423	1.443	1.489	(1.441)	SC	0.7	Y-Γ/Y-Γ

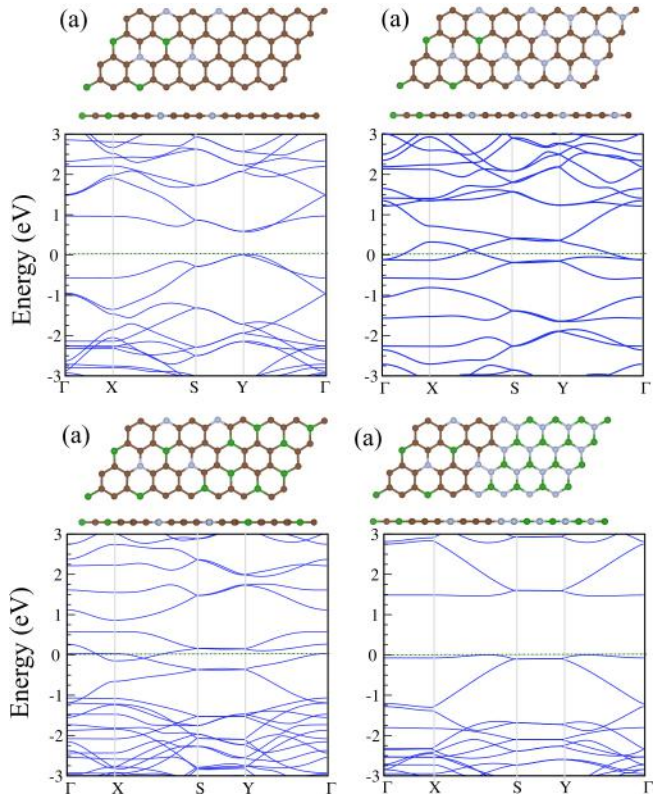

Figure 3: Optimized atomic structures (top) and electronic band structure (bottom) of (a) Gr-dop@Gr, (b) C_3N-dop@Gr, (c) BC_3-dop@Gr, (d) BN-dop@Gr HTJs. The energy is calculated relative to the Fermi energy.

in Figs. 2(a-d). The obtained parameters for the lattice constant (a), interlayer distance (h) and other parameters of the studied HTS are listed in Table 1. The bond lengths of C-C and B-N are 1.421 and 1.442 Å, respectively, which are slightly larger than that of the pristine BN monolayer. The interlayer distance between two monolayer planes is 3.553 Å. The interlayer distance between dop@Gr and different single layers are about 3.326-3.384 Å, which is typical of vdW equilibrium spacing. The difference charge densities of the studied HTSs are shown in the right of optimized structure (top) in Fig. 2. The blue and yellow colors indicate gain and loss charge electron density. A high charge density distributes around the B atom which indicates a charge transfer from C and N atoms to B atom resulting in covalent bonding. The AIMD calculation of C_3N/dop@Gr was accomplished using the canonical NVT ensemble at 300K for 3ps, as shown inFig. S3. The thermal stability was validated by the time-dependent calculation of temperature. The snapshots of the structure show that the atoms are displaced around their equilibrium positions throughout the simulations. Furthermore, neither broken bond nor structural reconstruction takes place at 300 K, demonstrating the thermal stability of designed structure at room temperature.

The band structures with the corresponding DOS and PDOS of the studied HTSs within PBE functional are illustrated in Figs. 2(a-d). For Gr/dop@Gr, the Dirac-point of the structure is not the same as in Gr monolayer and the structure has a direct bandgap of 0.1 eV which is smaller than that of dop@Gr bandgap (1.2 eV). The VBM is mainly derived from the C-p_z states of Gr and C-p_z states of dop@Gr, while CBM is derived from C-p_z orbitals of Gr (see PDOS in Fig. 2(a)). Regarding C_3N/dop@Gr, the strong interaction between dop@Gr and C_3N induces a metallic character of the HTSs. PDOS shows the metallic character near the Fermi energy comes from C-p_z states of C_3N layer (see Fig. 2(b)). Figure 2(c) shows the BC_3/dop@Gr is a direct semiconductor Γ-point with a small bandgap of 80 meV. For BN/dop@Gr HTS, the bandgap is 1.23 eV which is more related to the bandgap of dop@Gr. The contribution of B and C states (p_z) in the CBM is dominant, while the VBM is dominated by N-p_z. Due to the direct bandgaps of the monolayers, the HTS has also a direct bandgap at K-point (see Fig. 2(d)). Since the PBE approach underestimate the electronic band gap, the HSE06 [60] functional was also used to evaluate the electronic band structure as depicted in Fig. S4. It is found that the HSE06 functional does not change the bang gap of Gr/dop@Gr structure whereas it opens the electronic band gap of other hetrostructures in comparison with PBE. Based on the acquired band structure by HSE06 method, the indirect band-gaps of C_3N/dop@Gr was estimated to be 0.44 eV. For this structure the VBM is located at -point while the CBM is situated at K-point. The HSE06 approach changes the value and sort of semiconducting band gap for BC_3/dop@Gr system. The band gap value for BC_3/dop@Gr hetrostructure predicted to be 0.21eV on the basis of HSE06 results where the VBM and CBM locate at K- and Γ-point, respectively, resulting in an indirect band gap. Nevertheless, the HSE06 approach does not change the sort of direct semiconducting band gap in BN/dop@Gr system. The band gap value for this system is 1.77 eV within HSE06 approach.

4.1. Heterojunctions

By sticking Gr, C_3N, BC_3, BN monolayers to dop@Gr laterally, four HTJs are created. The optimized structures and the corresponding band structures of Gr-dop@Gr, C_3N-dop@Gr, BC_3-dop@Gr and BN-dop@Gr HTJs are shown in Figs. 3(a-d). The lattice parameters, the bond lengths, and the bandgap of HTJs are tabulated in Table 2. The Gr-dop@Gr is a semicon-

ductor with a direct bandgap of 0.4 eV which is smaller than the bandgap of dop@Gr due to the increase of the C concentration. The VBM and CBM are located at the Y-Γ path. When the C_3N monolayer stacks with dop@Gr sheet, the concentration of N increases as compared to the concentration of B in the HTJ. Therefore, the HTJ behave as n-type conducting due to the extra charge of the N atoms as compared to B atoms (Fig. 3(d))). However, the concentration of B atoms is larger than the concentration of N atoms in the BC_3-dop@Gr HTJ, therefore, its character is p-type conducting (Fig. 3(b) and Fig. 3(c)). Regarding BN-dop@Gr HTJ (Fig. 3(d))), the bandgap becomes 0.7 eV which is smaller than the bandgap of BN and dop@Gr sheets. The decrease of the HTJ bandgap can be attributed to the increasing of C concentration in the BN sheets. The HSE06 results predict the semiconductiong properties for Gr-dop@Gr and BN-dop@Gr heterojunction systems and metallic character for C_3N-dop@Gr and BC_3-dop@Gr systems (Fig. S5). Our results show that the Gr-BN@Gr is a semiconductor with a direct band gap of 0.84 eV at Y-point. Our results also show a direct band gap character with the value of 1.47 eV which the VBM and CBM lie on the X-S path.

5. Optical properties

To understand the optical properties of considered heterostructures and heterojunctions, the absorption coefficient of monolayers of the components for these structures is calculated. Fig. 4(a) shows Gr/(-)dop@ Gr, a wide absorption peak appears at 275 nm for both heterostructures and heterojunctions, which can be attributed to the contributions of both monolayers. The number of peaks above 300 nm for HTS is larger than the corresponding number for HTJ. The HTS and HTJ can enhance ultraviolet absorption as compared to the monolayers. The HTS absorbs a wide range of visible light more than the monolayers and HTJ. In the whole wavelength range the light absorption of the HTS is larger than of the HTJ due to the atomic thickness of the HTJ. Regarding C_3N/dop@Gr, the absorption of the HTS is related to the absorption of the dop@Gr layer below 440 nm and above that is related to the absorption of C_3N sheet. For C_3-dop@Gr, the optical properties are related to the combination of the monolayers in the whole wavelength range (see Fig. 4(b)). The HTS is a good candidate to absorb a wide range of visible light as compared to the graphene sheet and HTJ. The absorption spectrum of BC_3/(-)dop@Gr is very similar to the corresponding C_3N/(-)dop@Gr (see Fig. 4(c)). For BN/(-)dop@Gr, Fig. 4(d) , the are many pronounced peaks in the range of 220 nm to 320 nm, the BN layer decreases the broadening of the absorption peaks as compared to the Gr monolayer (see Fig. 4(d)). The absorption spectrum of the BN layer is vanishing above 290 nm therefore the absorption of the HTS is more related to the absorption of the dop@graphene layer. The absorbing light for BN/(-)dop@ Gr is less than of Gr/(-)dop@Gr, except at 220 nm, due to the smaller bandgap of Gr/(-)dop@Gr as compared to BN/(-)dop@ Gr. The optical properties of HTS and HTG are well explained in terms of a superposition of the corresponding monolayers. The HTS and HTJ which include Gr or BN can enhance the absorption of light as compared to the absorption of Gr or BN monolayers in the whole wavelength range. For HTS and HTJ which contain C_3 N or BC_3 can enhance the absorption in the ultra-violet wavelengths as compared to the absorption of C_3 N and BC_3 monloayers.

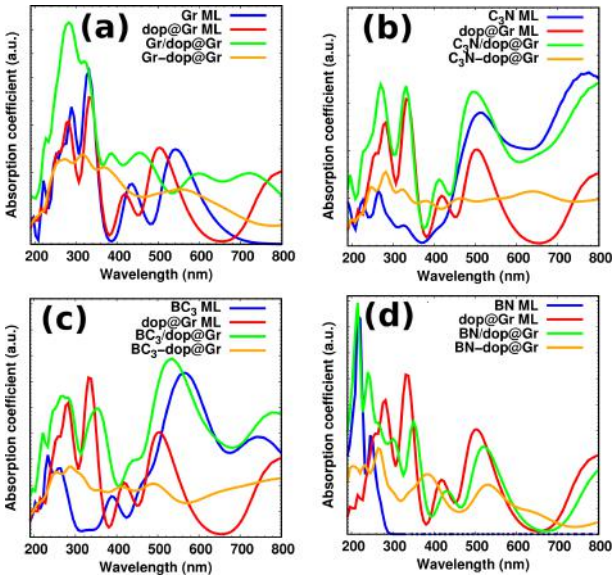

Figure 4: Absorption spectrum of (a) Gr/(-)dop@Gr, (b) C_3N/(-)dop@Gr, (c) BC_3/(-)dop@Gr, and (d) BN/(-)dop@ Gr heterostructures (/) and heterojunctions (-).

6. Electric field effect

With regard to potential device applications, the ability to tune the electronic structure by e.g. controlling the Fermi-level via electric field (F) is highly desirable. The presence of the interlayer distance in Gr/dop@Gr leads to a potential difference between the two atomic layers, which is intrinsically useful in tunable the electronic properties. In the following paragraph, the effect of E-field on the electronic properties of the heterostructure is investigated. The strength of the F >0 (<0) denotes parallel (antiparallel) to the z-axis. The electronic band structure of Gr/, C_3N/, BC_3/ and BN/dop@Gr in the presence of a perpendicular F are shown in Figs. 5(a-c). The variation of the bandgap as a function of the E-field is shown in Figs. 5(e,f). The electronic structure is strongly modified by applying the E-field. With applying a parallel E-field (F>0) in Gr/dop@Gr, direct bandgap decreases from 0.12 eV (0 V/Å) to 20 meV (0.4 V/Å). Surprisingly, further increase of the electric field to 0.6 V/Å, the bandgap increases and a dual indirect bandgaps of ~50 meV is created (Fig. 5(a)). The increase of F from 0.6 to 1 V/Å, the dual bandgap is maintained at about 50-80 meV. The electronic response of Gr/dop@Gr in the anti-parallel direction (F<0) differs from that in the parallel direction. Specifically, the negative E-field increases the bandgap to 0.20 eV (at 0.2 V/Å), 0.30 eV (at 0.4 V/Å), 0.33 eV (at 0.5 V/Å). Interestingly, the bandgap reaches 0.35 eV at 0.6 V/Å and for further increase of the E-field to 1 V/Å, the shape of dual narrow bandgap is preserved. For the E-field varying from 0.6 to 1 V/Å, the bandgap stays the same.

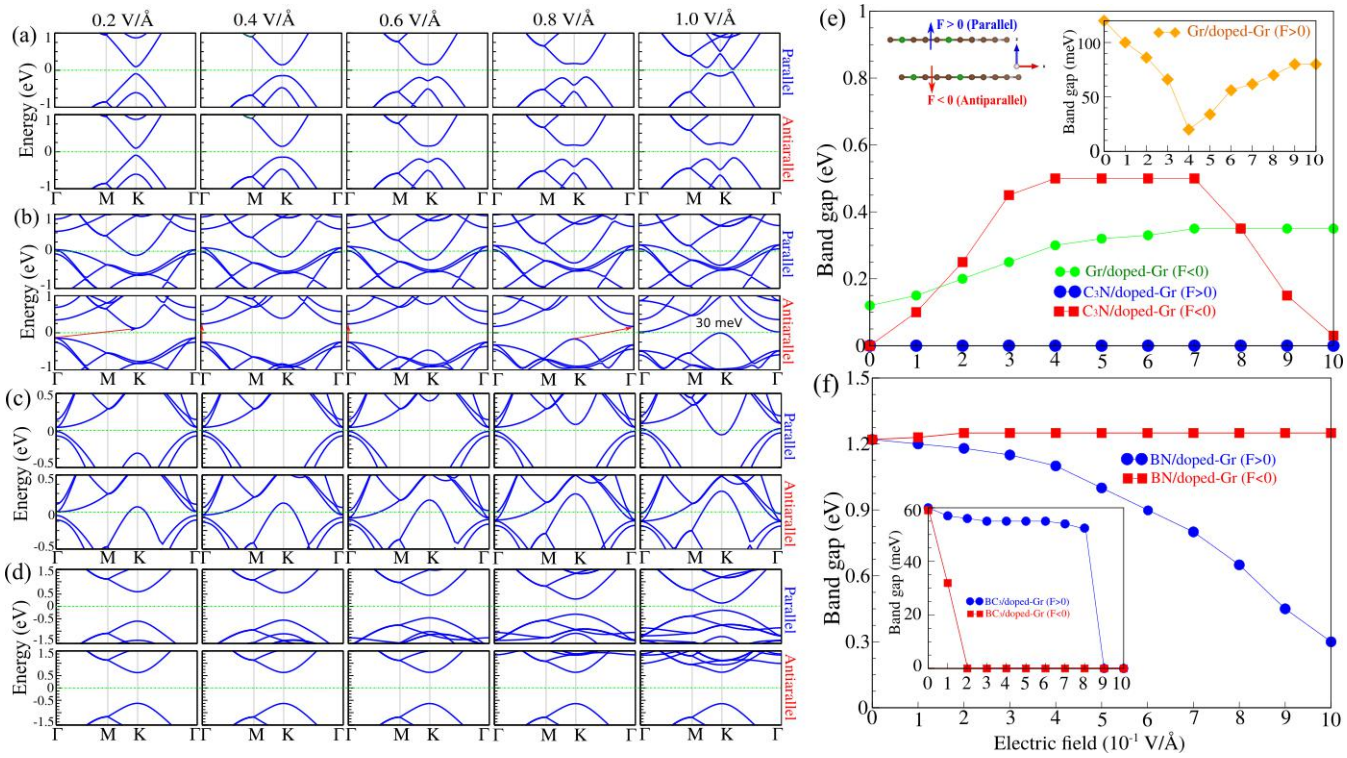

Figure 5: Electronic band structures of (a) Gr/dop@Gr, (b) C_3N/dop@Gr, (b) BC_3/dop@Gr and (d) BN/dop@Gr HTSs, as a function of applied electric field in the parallel (top) and anti-parallel (bottom) directions. The positive (negative) electric field refers to parallel (antiparallel) to the z-axis in the normal direction, where the strength of fields varies from 0 to 1 V/Å. The energy is calculated relative to the Fermi energy. (e,d) Variation of bandgap as a function of applied electric field.

When the applied filed on C_3N/dop@Gr increases, F>0 (0.1-1 V/Å), the crossing bands at the Fermi-level increases (Fig. 5(b)). In the case of opposite fileds, F<0 regime, the situation is completely different from F>0. The E-field opens a bandgap in the C_3N/dop@Gr structure. When the applied negative E-field reaches to 0.1 and 0.2 V/Å a metal-to-semiconductor transition occurs and the indirect bandgaps are calculated 0.1 and 0.25 eV, respectively. Interestingly, when the applied field becomes 0.4 V/Å, the indirect bandgap transforms to direct bandgap of 0.5 eV. When the E-field changes from 0.5 to 0.7 V/Å, the bandgap stays without any change. At higher fields (F= 0.8 V/Å to F = 1 V/Å), the bandgap becomes indirect and decreases as the field increases (Fig. 5(c)). The BC_3/dop@Gr is a semiconductor with a small bandgap 60 meV in absence of E-field. For parallel applied field, the bandgap (0.55 eV) does not change when the strength changes from 0.2 V/Åto 0.8 V/Å. The electronic structure of BC_3/dop@Gr changes to metallic system in the range of 0.9 V/Å. Regarding the reverse direction of the applied filed, the bandgap decreases to 30 meV at 0.1 V/Å and for higher fields the HTS becomes a metallic structure. The BN/dop@Gr is a semiconductor with a direct bandgap 1.22 eV (at 0.0 V/Å). The bandgap decreases as the forward applied filed increases. However, for reverse applied field, the bandgap increases to 1.25 eV for fields larger than or equal 0.2 V/Å (Fig. 5(d)). Thus, the electric field tunes the electronic properties over a wide range for doped-graphene based HTSs which can lead to important applications in nanoscale electronic and opto-electronic devices.

7. Pressure effect

The impact of vertical strain on the band structure of the HTSs is studied by decreasing or increasing the vertical distance between the two monolayers. The strain is defined as $\varepsilon = (h \pm h_0)/h_0$, where h and h_0 are the equilibrium and fixed interlayer distances, respectively. Fig. 6(a) left-hand side (right-hand side) shows the influence of negative (positive) vertical strain on the Gr/dop@Gr. The change in the bandgap is very large for Gr/dop@Gr under the strain, where the bandgap is 85 meV at 3.235 Å and decreases to 30 meV at 3.735 Å. For C_3N/dop@Gr, at higher negative strain (2.926 Å), the CBM at K-point is shifted towards the Fermi energy and a narrow bandgap of 45 meV is opened, i.e., the structure becomes a semiconductor (Fig. 6(b) (left-hand side)). In contrast, the positive strain does not affect the band structure (Fig. 6(b) (right-hand side)). The positive vertical strain has a significant influence on the band structure of BC_3/dop@Gr (right of Fig. 6(c)). At distances of 3.374 Å and 3.474 Å, the indirect bandgaps are 80 meV and 35 meV, respectively. Interestingly, a higher positive strain (3.474 Å), moves the VBM towards the Fermi energy and closes the bandgap, i.e., the HTS becomes a metallic system. As the negative strain increases the bandgap increases too (left of Fig. 6(c)). One can find that the suitable bandgap values can be achieved at various interlayer distances. For the BN/dop@Gr, the interlayer coupling tunes the bandgap of BN/dop@Gr and the bandgaps ranging from 1.2 eV-1.05 eV (negative strain) and 1.24 eV-1.3 eV (positive strain) can be achieved at various interlayer distances.

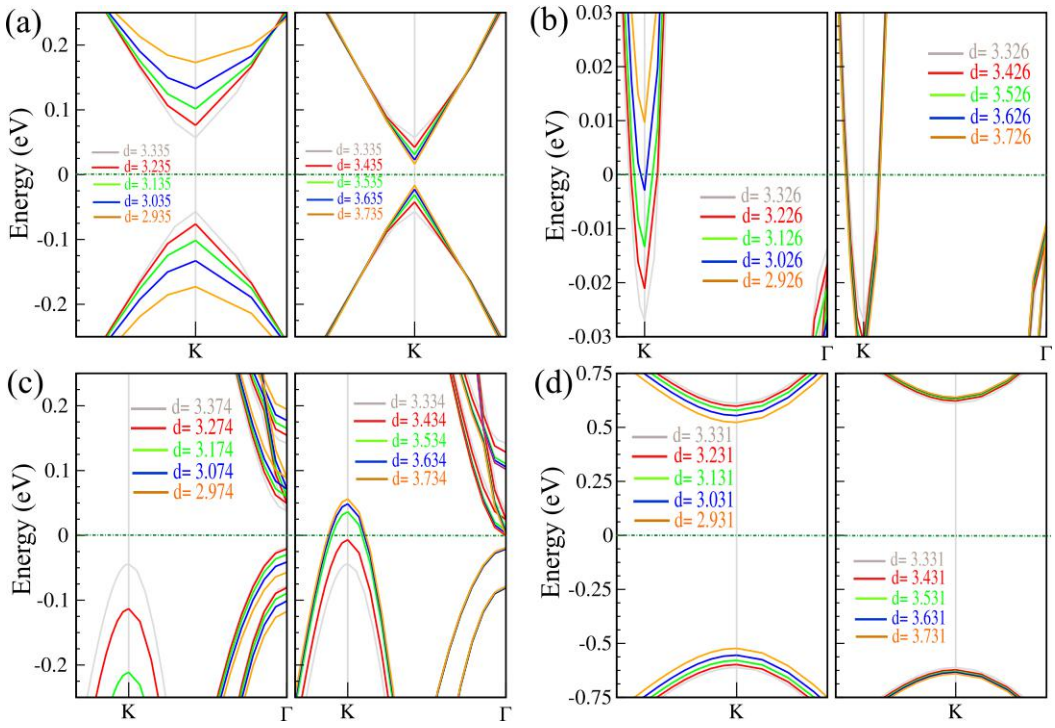

Figure 6: Electronic band structure of (a) Gr/dop@Gr, (b) C_3N/dop@Gr, (b) BC_3/dop@Gr and (d) BN/dop@Gr HTS with respect of compressive (left) and tensile (right) interlayer distance. The energy is calculated relative to the Fermi energy.

8. Conclusion

A systematic investigation of the electronic and optical properties of van der Waals vertical heterostructures and lateral heterojuctions between dop@Gr and Gr, Gr-like C_3N, BC_3 and h-BN monolayers employing DFT calculations has been performed. Our results demonstrate that the dop@Gr/Gr, C_3N/dop@Gr, BC_3/dop@Gr and BN/dop@Gr HTSs are energetically and thermally feasible at room temperature, therefore the heterostructures can be synthesized experimentally, which is an important achievement of our study. The Gr/-dop@Gr, BN/-dop@Gr HTSs and HTJs exhibit the semiconducting nature. While the C_3N with dop@Gr HTS and HTJ are metallic states because of the strong interaction between the two monolayers, the formation of HTJ between BC_3 and dop@Gr tends to a transition from a semiconductor in dop@Gr/BC_3 HTS to a metal in BC_3-dop@Gr. The absorption spectra of the heterostructures reveal that the HTSs have ability to absorb the visible light more effectively than the corresponding monolayers. The impacts of the electric field and pressure on the electronic properties of these HTS are also investigated. The bandgap modification of these HTSs and HTJs by applying an electric field and by pressure strain is demonstrated.

9. CRediT authorship contribution statement

A. Bafekry: Conceptualization, Data curation, Formal analysis, Funding acquisition, Investigation, Methodology, Project administration, Resources, Software, Supervision, Validation, Visualization, Writing - original draft, Writing - review and editing. D. Gogova: Validation, Writing - review and editing. M. M. Fadollah: Validation, Visualization, Formal analysis, Data curation, Software, Writing - review. C. Nguyen: Validation, Writing - review and editing. M. Faraji: review and editing. M. Ghergherehchi: Validation, Visualization, Writing - review and editing. M. Oskoeian: review and editing.

10. Declaration of competing interest

The authors declare that they have no known competing financial interests or personal relationships that could have appeared to influence the work reported in this paper.

11. Acknowledgments

This work was supported by the National Research Foundation of Korea (NRF) grant funded by the Korea government (MSIT) (NRF-2017R1A2B2011989). In addition, this research is funded by Vietnam National Foundation for Science and Technology Development (NAFOSTED) under grant number 103.01-2019.05.

[1] Hong T. T. Nguyen, Mohammed M. Obeid, Asadollah Bafekry, M. Idrees, Tuan V. Vu, Huynh V. Phuc, Nguyen N. Hieu, Le T. Hoa, Bin Amin, and Chuong V. Nguyen. Interfacial characteristics, schottky contact, and optical performance of a graphene/ga_2SSe van der waals heterostructure: Strain engineering and electric field tunability. Phys. Rev. B, 102:075414, Aug 2020.

[2] Zhinan Ma, Bo Wang, Liangkai Ou, Yan Zhang, Xu Zhang, and Zhen Zhou. Structure and properties of phosphorene-like IV-VI 2D materials. Nanotechnol., 27(41):415203, 2016.

[3] Kin Fai Mak, Changgu Lee, James Hone, Jie Shan, and Tony F Heinz. Atomically thin MoS2: a new direct-gap semiconductor. Phys. Rev. Lett., 105(13):136805, 2010.

[4] Jia-He Lin, Hong Zhang, Xin-Lu Cheng, and Yoshiyuki Miyamoto. Single-layer group IV-V and group V-IV-III-VI semiconductors: Structural stability, electronic structures, optical properties, and photocatalysis. Phys. Rev. B, 96(3):035438, 2017.

[5] Alexandra Carvalho, Min Wang, Xi Zhu, Aleksandr S Rodin, Haibin Su, and Antonio H Castro Neto. Phosphorene: from theory to applications. Nat. Rev. Mater., 1(11):1–16, 2016.

[6] Haining Wang, Changjian Zhang, Weimin Chan, Sandip Tiwari, and Farhan Rana. Ultrafast response of monolayer molybdenum disulfide photodetectors. Nat. Commun., 6(1):1–6, 2015.

[7] Vitaly Podzorov, ME Gershenson, Ch Kloc, R Zeis, and E Bucher. High-mobility field-effect transistors based on transition metal dichalcogenides. Appl. Phys. Lett., 84(17):3301–3303, 2004.

[8] Saptarshi Das, Marcel Demarteau, and Andreas Roelofs. Ambipolar phosphorene field effect transistor. ACS Nano, 8(11):11730–11738, 2014.

[9] Sajedeh Manzeli, Dmitry Ovchinnikov, Diego Pasquier, Oleg V Yazyev, and Andras Kis. 2D transition metal dichalcogenides. Nat. Rev. Mater., 2(8):17033, 2017.

[10] Congpu Mu, Jianyong Xiang, and Zhongyuan Liu. Photodetectors based on sensitized two-dimensional transition metal dichalcogenides-a review. J. Mater. Res., 32(22):4115–4131, 2017.

[11] Nourdine Zibouche, Agnieszka Kuc, Janice Musfeldt, and Thomas Heine. Transition-metal dichalcogenides for spintronic applications. Ann. der Phys., 526(9-10):395–401, 2014.

[12] Lídia C Gomes and A Carvalho. Phosphorene analogues: Isoelectronic two-dimensional group-IV monochalcogenides with orthorhombic structure. Phys. Rev. B, 92(8):085406, 2015.

[13] Zhen Tian, Chenglei Guo, Mingxing Zhao, Ranran Li, and Jiamin Xue. Two-dimensional SnS: a phosphorene analogue with strong in-plane electronic anisotropy. Acs Nano, 11(2):2219–2226, 2017.

[14] Han Liu, Adam T Neal, Zhen Zhu, Zhe Luo, Xianfan Xu, David Tománek, and Peide D Ye. Phosphorene: an unexplored 2D semiconductor with a high hole mobility. ACS Nano, 8(4):4033–4041, 2014.

[15] Shubin Yang, Yongji Gong, Jinshui Zhang, Liang Zhan, Lulu Ma, Zheyu Fang, Robert Vajtai, Xinchen Wang, and Pulickel M Ajayan. Exfoliated graphitic carbon nitride nanosheets as efficient catalysts for hydrogen evolution under visible light. Adv. Mater., 25(17):2452–2456, 2013.

[16] Qinghua Liang, Zhi Li, Zheng-Hong Huang, Feiyu Kang, and Quan-Hong Yang. Holey graphitic carbon nitride nanosheets with carbon vacancies for highly improved photocatalytic hydrogen production. Adv. Funct. Mater., 25(44):6885–6892, 2015.

[17] Cory R Dean, Andrea F Young, Inanc Meric, Chris Lee, Lei Wang, Sebastian Sorgenfrei, Kenji Watanabe, Takashi Taniguchi, Phillip Kim, Kenneth L Shepard, et al. Boron nitride substrates for high-quality graphene electronics. Nat. Nanotechnol., 5(10):722–726, 2010.

[18] Branimir Radisavljevic, Aleksandra Radenovic, Jacopo Brivio, Valentina Giacometti, and Andras Kis. Single-layer MoS2 transistors. Nat. Nanotechnol., 6(3):147, 2011.

[19] Javeed Mahmood, Eun Kwang Lee, Minbok Jung, Dongbin Shin, In-Yup Jeon, Sun-Min Jung, Hyun-Jung Choi, Jeong-Min Seo, Seo-Yoon Bae, So-Dam Sohn, et al. Nitrogenated holey two-dimensional structures. Nat. Commun., 6:6486, 2015.

[20] Bohayra Mortazavi. Ultra high stiffness and thermal conductivity of graphene like C3N. Carbon, 118:25–34, 2017.

[21] Xinchen Wang, Kazuhiko Maeda, Arne Thomas, Kazuhiro Takanabe, Gang Xin, Johan M Carlsson, Kazunari Domen, and Markus Antonietti. A metal-free polymeric photocatalyst for hydrogen production from water under visible light. Nat. mater., 8(1):76–80, 2009.

[22] A. Bafekry, M. Yagmurcukardes, M. Shahrokhi, and M. Ghergherehchi. Electro-optical properties of monolayer and bilayer boron-doped c3n: Tunable electronic structure via strain engineering and electric field. Carbon, 168:220 – 229, 2020.

[23] Javeed Mahmood, Eun Kwang Lee, Minbok Jung, Dongbin Shin, Hyun-Jung Choi, Jeong-Min Seo, Sun-Min Jung, Dongwook Kim, Feng Li, Myoung Soo Lah, et al. Two-dimensional polyaniline (C3N) from carbonized organic single crystals in solid state. PNAS, 113(27):7414–7419, 2016.

[24] Siwei Yang, Wei Li, Caichao Ye, Gang Wang, He Tian, Chong Zhu, Peng He, Guqiao Ding, Xiaoming Xie, Yang Liu, et al. C3NA 2D crystalline, hole-free, tunable-narrow-bandgap semiconductor with ferromagnetic properties. Adv. Mater., 29(16):1605625, 2017.

[25] Asadollah Bafekry, Saber Farjami Shayesteh, and Francois M Peeters. C3N monolayer: Exploring the emerging of novel electronic and magnetic properties with adatom adsorption, functionalizations, electric field, charging, and strain. J. Phys. Chem. C, 123(19):12485–12499, 2019.

[26] Li-Bin Shi, Yan-Yan Zhang, Xiao-Ming Xiu, and Hai-Kuan Dong. Structural characteristics and strain behavior of two-dimensional C3N: First principles calculations. Carbon, 134:103–111, 2018.

[27] A. Bafekry, C. Nguyen, M. M. Obeid, and M. Ghergherehchi. Modulating the electro-optical properties of doped c3n monolayers and graphene bilayers via mechanical strain and pressure. New J. Chem., 44:15785–15792, 2020.

[28] A Bafekry and M Neek-Amal. Tuning the electronic properties of graphene–graphitic carbon nitride heterostructures and heterojunctions by using an electric field. Phys. Rev. B, 101(8):085417, 2020.

[29] Bingling He, Jiansheng Shen, Dongwei Ma, Zhansheng Lu, and Zongxian Yang. Boron-doped C3N monolayer as a promising metal-free oxygen reduction reaction catalyst: a theoretical insight. J. Phys. Chem. C, 122(35):20312–20322, 2018.

[30] Li-Bin Shi, Mei Yang, Shuo Cao, Qi You, Ya-Jing Zhang, Meng Qi, Kai-Cheng Zhang, and Ping Qian. Prediction of high carrier mobility for a novel two-dimensional semiconductor of bc 6 n: first principles calculations. Journal of Materials Chemistry C, 8(17):5882–5893, 2020.

[31] Asadollah Bafekry, Saber Farjami Shayesteh, and Francois M Peeters. Two-dimensional carbon nitride (2dcn) nanosheets: Tuning of novel electronic and magnetic properties by hydrogenation, atom substitution and defect engineering. J. Appl. Phys., 126(21):215104, 2019.

[32] Shuo Cao, Mei Yang, Qi You, Li-Bin Shi, and Ping Qian. Theoretical evaluation of intrinsic mobility for two-dimensional semiconductor of bc2n: First-principles calculation. Physica E: Low-dimensional Systems and Nanostructures, 120:114062, 2020.

[33] Dandan Wang, Yu Bao, Tongshun Wu, Shiyu Gan, Dongxue Han, and Li Niu. First-principles study of the role of strain and hydrogenation on C3N. Carbon, 134:22–28, 2018.

[34] A Bafekry, C Stampfl, S Farjami Shayesteh, and FM Peeters. Exploiting the novel electronic and magnetic structure of C3N via functionalization and conformation. Adv. Electron. Mater., 5(12):1900459, 2019.

[35] A Bafekry, C Stampfl, and M Ghergherehchi. Strain, electric-field and functionalization induced widely tunable electronic properties in mos2/bc3,/c3n and/c3n4 van der waals heterostructures. Nanotechnology, 31(29):295202, 2020.

[36] Dongwei Ma, Jing Zhang, Yanan Tang, Zhaoming Fu, Zongxian Yang, and Zhansheng Lu. Repairing single and double atomic vacancies in a c3n monolayer with co or no molecules: a first-principles study. Physical Chemistry Chemical Physics, 20(19):13517–13527, 2018.

[37] A Bafekry, B Akgenc, S Farjami Shayesteh, and B Mortazavi. Tunable electronic and magnetic properties of graphene/carbon-nitride van der waals heterostructures. Appl. Surf. Sci., 505:144450, 2020.

[38] A. Bafekry and C. Stampfl. Band-gap control of graphenelike borocarbonitride $g-bc_6N$ bilayers by electrical gating. Phys. Rev. B, 102:195411, Nov 2020.

[39] Asadollah Bafekry, Catherine Stampfl, Chuong Nguyen, Mitra Ghergherehchi, and Bohayra Mortazavi. Tunable electronic properties of the dynamically stable layered mineral pt2hgse3 (jacutingaite). Phys. Chem. Chem. Phys., 22:24471–24479, 2020.

[40] Chunmei Zhang, Yalong Jiao, Tianwei He, Steven Bottle, Thomas Frauenheim, and Aijun Du. Predicting two-dimensional C3B/C3N van der Waals p–n heterojunction with strong interlayer electron coupling and enhanced photocurrent. j. Phys. Chem. lett., 9(4):858–862, 2018.

[41] Jun Zhao, Hui Zeng, and Xingfei Zhou. X3N (X= C and Si) monolayers and their van der Waals Heterostructures with graphene and h-BN: Emerging tunable electronic structures by strain engineering. Carbon, 145:1–9, 2019.

[42] Mohammed M. Obeid, Asadollah Bafekry, Sajid Ur Rehman, and Chuong V. Nguyen. A type-ii gase/hfs2 van der waals heterostructure as promising photocatalyst with high carrier mobility. Applied Surface Science, 534:147607, 2020.

[43] Asdollah Baafekry, Mehmet Yagmurcukardes, Berna Akgenc, Mitra Ghergherehchi, and Chuong Nguyen. Van der waals heterostructures

of mos2 and janus mosse monolayers on graphitic boron-carbon-nitride (bc3, c3n, c3n4 and c4n3) nanosheets: a first-principles study. J. Phys. D: Appl. Phys., 53(35), 2020.

[44] A. Bafekry, M. M. Obeid, Chuong V. Nguyen, M. Ghergherehchi, and M. Bagheri Tagani. Graphene hetero-multilayer on layered platinum mineral jacutingaite (pt2hgse3): van der waals heterostructures with novel optoelectronic and thermoelectric performances. J. Mater. Chem. A, 8:13248–13260, 2020.

[45] Jiantie Xu, Javeed Mahmood, Yuhai Dou, Shixue Dou, Feng Li, Liming Dai, and Jong-Beom Baek. 2D Frameworks of C2N and C3N as New Anode Materials for Lithium-Ion Batteries. Adv. Mater., 29(34):1702007, 2017.

[46] Yameng Zhao, Dongwei Ma, Jing Zhang, Zhansheng Lu, and Yuanxu Wang. Transition metal embedded c3n monolayers as promising catalysts for the hydrogen evolution reaction. Physical Chemistry Chemical Physics, 21(36):20432–20441, 2019.

[47] Dongwei Ma, Jing Zhang, Xinxin Li, Chaozheng He, Zhiwen Lu, Zhansheng Lu, Zongxian Yang, and Yuanxu Wang. C3n monolayers as promising candidates for no2 sensors. Sensors and Actuators B: Chemical, 266:664–673, 2018.

[48] Taisuke Ozaki, Kengo Nishio, and Hiori Kino. Efficient implementation of the nonequilibrium green function method for electronic transport calculations. Phys. Rev. B, 81:035116, Jan 2010.

[49] Hendrik J Monkhorst and James D Pack. Special points for brillouin-zone integrations. Phys. Rev. B, 13(12):5188, 1976.

[50] Stefan Grimme. Semiempirical GGA-type density functional constructed with a long-range dispersion correction. J. Comput. Chem., 27(15):1787–1799, 2006.

[51] Jose M Soler, Emilio Artacho, Julian D Gale, Alberto Garcia, Javier Junquera, Pablo Ordejon, and Daniel Sanchez-Portal. The SIESTA method forab initioorder-nmaterials simulation. J. Phy.: Condensed Matter, 14(11):2745–2779, mar 2002.

[52] D.R. Willians M. Bass, E.W.V. Stryland and W.L. Woffe. Handbook of Optics, secon edition, vol. 1. McGraw-Hill, New York, 1995.

[53] Amal Kasry, Mohamed M. Fadlallah, Nicolas H. Voelcker, and Ahmed A. Maarouf. Experimental and theoretical demonstrations of ultraviolet absorption enhancement in porous nano-membrane graphene. Carbon, 155:65 – 70, 2019.

[54] AH Castro Neto, Francisco Guinea, Nuno MR Peres, Kostya S Novoselov, and Andre K Geim. The electronic properties of graphene. Rev. modern phys., 81(1):109, 2009.

[55] Kostya S Novoselov, D Jiang, F Schedin, TJ Booth, VV Khotkevich, SV Morozov, and Andre K Geim. Two-dimensional atomic crystals. PNAS, 102(30):10451–10453, 2005.

[56] Javeed Mahmood, Eun Kwang Lee, Minbok Jung, Dongbin Shin, Hyun-Jung Choi, Jeong-Min Seo, Sun-Min Jung, Dongwook Kim, Feng Li, Myoung Soo Lah, et al. Two-dimensional polyaniline (C3N) from carbonized organic single crystals in solid state. PNAS, 113(27):7414–7419, 2016.

[57] Qianku Hu, Qinghua Wu, Haiyan Wang, Julong He, and Guanglei Zhang. First-principles studies of structural and electronic properties of layered C3N phases. physica status solidi (b), 249(4):784–788, 2012.

[58] HJ Xiang, Bing Huang, ZY Li, S-H Wei, JL Yang, and XG Gong. Ordered semiconducting nitrogen-graphene alloys. Phys. Rev. X, 2(1):011003, 2012.

[59] Somayeh Behzad. Mechanical control of the electro-optical properties of monolayer and bilayer BC3 by applying the in-plane biaxial strain. Surf. Sci., 665:37 – 42, 2017.

[60] J. Heyd and G. E. Scuseria. Efficient hybrid density functional calculations in solids: Assessment of the heydscuseriaernzerhof screened coulomb hybrid functional. J. Chem. Phys, 121:1187–1192, 2004.